Experimental characterization of rectangular-aperture acousto-optic deflectors: efficiency, bandwidth, and wavelength dependence

Author: Daniel Eloi Perrella Benítez
Facultat de Física, Universitat de Barcelona

Advisor: Jordi Tiana Alsina

Abstract: This work consists on the characterization of a rectangular-aperture acousto-optic deflector. The characterization is carried out using two different laser beams: Gaussian and elliptical. Furthermore, different wavelengths were used (488 nm, 561 nm, 637 nm). Several parameters of the AOD were measured: relative efficiency as a function of angular deflection, optimal angles of incidence, maximum bandwidth and optimal power and alignment to achieve maximum efficiency, all for different wavelengths.
Keywords: Acousto-optic deflector, rectangular-aperture, elliptical beam, Bragg diffraction.
SDGs: Quality education. Industry, innovation and infrastructure.

I. INTRODUCTION

The main goal of this work is to characterize an acousto-optic deflector with a rectangular-shaped aperture. More specifically, on the characterization of the first order deflection, which is the most intense one.

The use of a rectangular-aperture AOD is not arbitrary: the angular resolution and the number of resolvable points are determined by the aperture dimension along the acoustic wave propagation direction, which is the deflection axis [1]. Larger crystal dimensions for the orthogonal length, not only worsen the homogeneity of the acoustic wave, but also complicate the crystal fabrication process. Rectangular apertures maximize the effective aperture in the relevant direction, resulting in bigger bandwidth and angular resolution. This kind of AOD requires an anamorphic adaptation using cylindrical lenses (Fig. 2a).

The characteristics of these devices make them optimal to be implemented in advanced scanning systems, thereby increasing their field of view. The rectangular shaped AOD per se does not deflect more than a regular AOD, but it allows filling the pupil of any device to the fullest[1] [2]. Before the implementation of the AOD on any device, a full characterization is needed. This means, the optimal power, the efficiency angular dependence and the effective bandwidth were studied for different alignments and wavelengths.

The total deflection range of an AOD is determined by:

$$\Delta\theta_{\text{scan}} = \frac{\lambda\,\Delta f}{v} \tag{1}$$

Where Δf is the RF wave bandwidth, v is the sound wave speed and λ is the beam wavelength. It is important to highlight, that the deflection range does not depend on the aperture of the AOD, but only on the crystal material and the input RF frequencies.

Angular resolution ($\delta\theta$) depends on effective acoustic interaction length, and the number of resolvable points (N) can be estimated as:

$$\delta\theta \sim \frac{\lambda}{L_{\text{eff}}}, \qquad N \approx \frac{\Delta\theta_{\text{scan}}}{\delta\theta} \approx \frac{L_{\text{eff}}\,\Delta f}{v} \tag{2}$$

where λ is the beam wavelength, L_{eff} is the acoustic interaction effective length, Δf is the bandwidth and v is the speed of the sound wave inside the crystal. The number of resolvable positions is determined by the acoustic interaction length, which is equivalent to the aperture dimension along the deflection axis. As seen in (2), the dimensions of the aperture along the acoustic wave propagation direction determine the deflector resolution.

II. ACOUSTO-OPTIC DEFLECTORS

An acousto-optic deflector is a device that allows to deflect light at a certain angle. This angle is determined by the frequency of the sound wave applied by the transducer. Most AODs mainly consist of a crystal (TeO_2 for the studied AOD), a piezoelectric transducer and an acoustic absorber. The operation is simple: a radio-frequency signal is sent to the piezoelectric transducer, which makes it vibrate. This vibration is transmitted to the crystal as a sound wave. The successive wave fronts act as periodic planes within the crystal. When an incident beam interacts with these planes and satisfy Bragg's law, it diffracts at a specific angle. The RF signal determines the spacing between wave fronts, which modulates the crystal's refractive index and thus controls the deflection angle. Inside an AOD, Bragg's law is:

$$\sin(\theta_B) \approx \theta_B = \frac{\lambda}{2\Lambda} = \frac{\lambda}{2v} f \tag{3}$$

Where λ is the wavelength of the beam and Λ is the wavelength of the acoustic wave. Λ can be represented as $\Lambda = \frac{v}{f}$, where f is the frequency of the sound wave and v is its speed. The small-angle approximation is used, where $\sin(\theta) \approx \theta$. As we can see in (3), θ_B is proportional to not only f, but also λ. That's the reason why the deflection angle of a certain fixed frequency will change for different wavelengths. The speed of the sound wave was fixed at $v = 660\,m/s$. The expression for the AOD peak maximum efficiency is:

$$\eta = sin^2\left\{\frac{\pi}{\lambda_o cos\theta}\left[\frac{M_2 L}{2H} P_a\right]^{\frac{1}{2}}\right\} \tag{4}$$

This equation is only valid when the Bragg condition is fulfilled. In practice, once the incidence angle is fixed, changing the frequency drives the system away from the ideal angle, this deviation is called momentum mismatch (Δk_m). Theoretically, out of the Bragg condition, the efficiency should drop to zero. Only when the frequency is correct, a single delta function should be found. However, the interaction with the acoustic wave, generates a diffraction pattern, leading to measurable efficiency beyond the Bragg condition:

$$\eta_{real} = \eta_{max} \cdot sinc^2 \left(\frac{\Delta k_m L}{2\pi} \right) \quad (5)$$

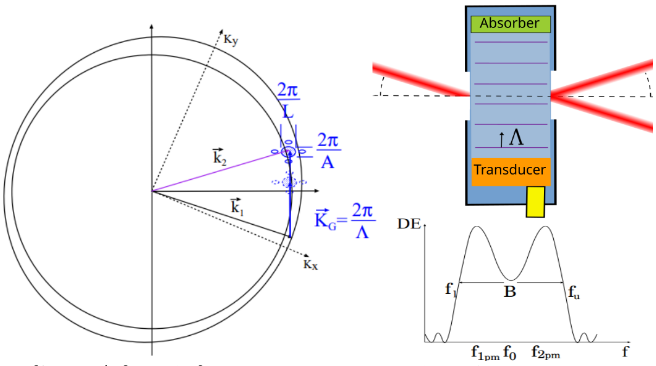

FIG. 1: AOD deflections represented with wave vectors, AOD device, and theoretical efficiency curve outside the ideal Bragg condition. [3]

The mentioned equations can be seen represented in Fig.1, as the theoretical efficiency curve shows two peaks that clearly behave as predicted by (5), placed at two frequencies that fulfill (3).

Another important parameter is the power of the RF wave sent to the AOD transducer. In fact, there is an optimal power for every mode and wavelength. For example, for the same wavelength (488 nm) the maximum efficiency on the single-frequency mode will be achieved with a low input power. Instead, hologram mode will require a much higher one. This idea will be expanded and shown in the results (Fig 4).

III. METHODOLOGY AND EXPERIMENTAL SETUP

The AOD manufacturer is Brimrose Corporation and its model is TED20-100-50-488/AR. The manufacturer of the remaining setup components is THORLABS, and will be referenced when first mentioned.

To characterize the AOD, both Gaussian and elliptical beams have been used (Fig. 2b). The Gaussian beam, as a reference, and the elliptical beam for the characterization itself. The elliptical beam is simply the expansion of the Gaussian beam along thex-axis. The use of the elliptical beam is interesting in itself since it covers the whole surface of the AOD aperture.

The experimental setup shown in Fig.3, consists on three main building blocks with different functions: the collimator, the beam expander and the AOD. It begins with an optical fiber (P3-405BPM-FC) coupled to a fiber adapter (SM1FC). At a distance of 19 mm, a converging lens (AC127-019-A-ML) with a focal length of $f' = 19$ mm is placed so that rays from the point source are collimated. This first segment of the setup generates the Gaussian beam and will be referred to as the "collimator".

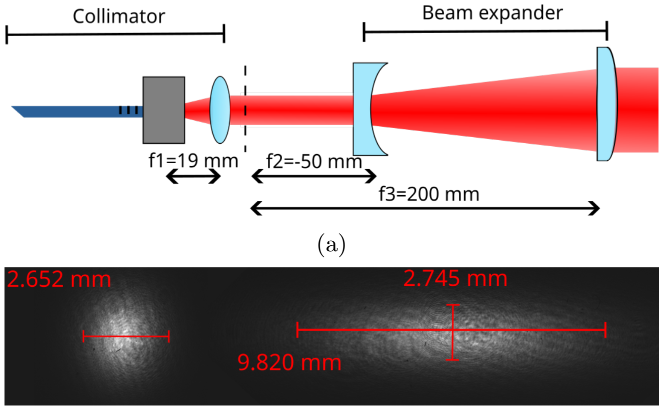

(b)

FIG. 2: (a)Collimator and beam expander. (b)Gaussian and elliptical beams for 488 nm.

After the collimator, the second building block is placed, which consists of an anamorphic Galilean telescope. The first telescope lens (LK1336RM-A), placed at an arbitrary distance from the collimator, is divergent and cylindrical, with a focal length of $f' = -50$ mm, and oriented parallel to thex-axis. This orientation causes the beam to expand along thex-axis. The second lens (LJ1653RM-A) is cylindrical and convergent, with a focal length of $f' = 200$ mm, also oriented parallel to thex-axis. This lens is at a distance of 150 mm from the first lens, in such a way that the focal lengths of the two lenses coincide. This makes the beam collimated, elliptical, and of a size suitable for the next assembly. The magnifications for this system are, on thex-axis:

$$\frac{\phi_{out}}{\phi_{in}} = -\frac{f'_{obj}}{f'_{ocu}} = \frac{200}{50} = 4 \quad (6)$$

This block of the set-up generates the elliptical beam (Fig. 2a). From now on will be referred as "beam expander". The beam diameters have been measured:

	Gaussian	Elliptical	
λ (nm)	Diameter (mm)	Major axis (mm)	Minor axis (mm)
488	2.652	9.820	2.745
561	2.504	8.970	2.534
637	2.229	8.227	2.298

The third building block of the set-up includes the acousto optic deflector, and an optional anamorphic relay. At an arbitrary distance of the collimator and the beam expander, the AOD is placed. The AOD used for the experiment has a rectangular window (3x14 mm), similar to the elliptical beam dimensions. After the AOD, the beam is deflected in multiple orders. For simplicity only the zero and first orders will be considered, since higher order deflections have negligible intensity.

A converging lens (LA1608-A-ML, $f = 75$ mm) is placed with the AOD pivot plane at its object focal plane.

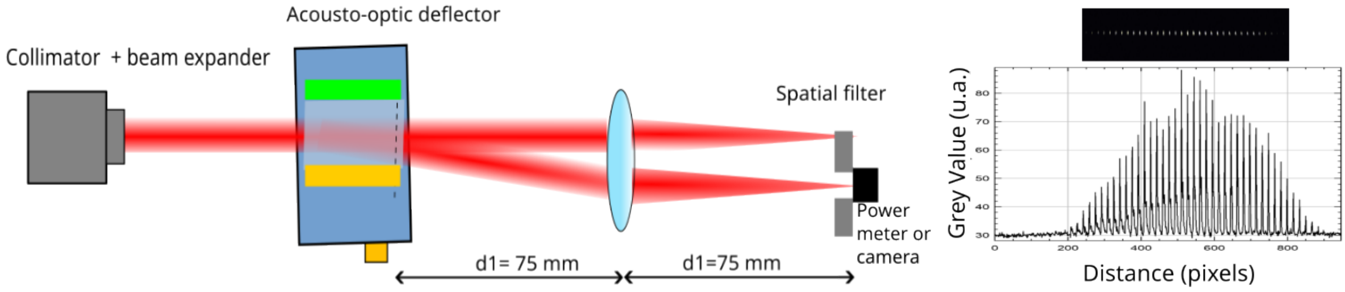

FIG. 3: Left: full set-up. Right: hologram created with GS algorithm with focused beam, and intensity profile.

This configuration converts the angular deflections produced by the AOD into positions, and the collimated beam spots are focused at the image focal plane. The beam enters the AOD collimated and linearly polarized along the x-axis. Finally, a spatial filter is used to remove the zero order. The spatial filter is a key item, because it allows us to only measure the first order diffraction . This set-up is optimal to measure efficiency curves. Despite this, a second lens ($f' = 30$ mm) can be added at a distance $d = 30$ mm of the spatial filter, creating an anamorphic relay, and conjugate the pivot point with the focal plane of the second lens. The inclusion of a relay is sub-optimal in terms of AOD characterization, but the use of the relay is necessary for the implementation of the AOD in other devices.

The alignment procedure of the AOD consists on manually moving and rotating the device to maximize the first-order deflected power, which means finding the ideal incidence angle. The ideal incidence angle is defined as the angle that maximizes the efficiency of the first order curve and results in a proper curve shape. The ideal incidence angles are optimized under broadband excitation conditions, since the objective is to maximize the diffraction efficiency over the widest possible frequency range rather than at a single frequency. To measure the ideal incidence angles, a detection screen is set at a certain distance from the AOD. Knowing the distance to the screen (d), and the distance between the beam origin and the reflected spot on the screen (h) allows us to calculate the ideal incidence angle as:

$$\theta = \frac{1}{2} arctan(\frac{h}{d}) \qquad (7)$$

The main characterization procedure consists on measuring efficiency curves, which measure the dependence between the deflection angle and the intensity of the deflected beam, $\eta(\theta)$. Not all curves satisfy the requirements we are looking for. To achieve a large FOV, the curve must have a wide bandwidth, good overall efficiency, and be flat on the top, so the illumination at every deflected angle is similar. Besides, it must be generated with an elliptical beam to fill the whole AOD aperture. For every wavelength, many parameters of the AOD will change, the most important one being the optimal alignment that maximizes the efficiency of the first order, but also the maximum achievable bandwidth, efficiency-frequency dependence, and the optimal power of the RF wave sent to the transducer. This is why most parameters will be studied for the three different wavelengths.

To plot the efficiency curve, a loop is programmed, where different frequencies are input to the AOD. This results in different powers captured by the detector, each one corresponding to a certain frequency. The efficiency is calculated as the ratio of deflected power to total power measured after the AOD. This represents the percentage of light that is deflected to the first order. By relating each efficiency to its corresponding frequency, $\eta(\theta)$ can be plotted.

The AOD operates in three deflection modes. In the "single-frequency" mode, a periodic RF signal is applied to the transducer, producing an acoustic wave at a fixed frequency and resulting in a static beam deflection to a single position. In the "sweep" mode, a predefined set of n RF frequencies is selected and rapidly cycled. This causes the AOD to sequentially deflect the beam to n distinct positions; although the deflection occurs sequentially, the switching rate is sufficiently high that the illumination appears simultaneous to an external observer. The "hologram" mode, uses the Gerchberg–Saxton algorithm [4], which iteratively retrieves a phase distribution to synthesize a target acoustic field, enabling the AOD to deflect the beam to all desired positions simultaneously.

Different modes require different optimal alignments and will result on different efficiency curves. For the single-frequency mode, only one position is being illuminated. Therefore, the efficiency curve shows a narrow bandwidth and a high efficiency on the optimized frequency. Instead, using the sweep or hologram modes will result on all the selected frequencies to benefit equally. The efficiency curve will be flatter and with a bigger bandwidth. Following the main objective of this work, the characterization will be done using the hologram and sweep modes.

To measure the hologram efficiency curve, a different method is needed. Since all deflections happen at the same time, relating each frequency to its intensity individually is not possible. This is why instead of a detector, a camera is used, and the intensity profile of the deflections is measured in grayscale values.

As a part of the set-up, the AOD programming was performed using Matlab. More specifically, the hologram mode has been created using the Gerchberg–Saxton algorithm. The intensity profile of the hologram and the beam dimensions have been measured using Fiji.

Multiple set-ups have been tested, including a second AOD device (AOD2). All experiments have also been tested by adding an anamorphic relay to the setup. The conclusion is that the best-performing AOD is AOD1 and the best way of characterization with the elliptical beam is not using the relay.

Since the transducer is an electronic device receiving a signal, some of the signal is accepted and some of it is not. The rejection of signals at certain frequencies, can diminish the power delivered by the transducer, reducing the efficiency. That's why a Vector Network Analyzer has been used to test the RF response (Fig.6).

IV. RESULTS

The AOD was aligned maximizing the measured power using the sweep mode, thus benefiting all frequencies equally and obtaining flatter efficiency peak with greater bandwidth. The optimal angles of incidence obtained using the method described in the previous section are:

	Optimal incidence angle (°)	
λ (nm)	Gaussian beam	Elliptical beam
488	3,211	3,455
561	3,085	3,315
637	3,065	3,295

θ has a relative error of 0.2%, calculated with the error propagation of III

To determine the optimal power, multiple saturation curves were measured. For the central frequency, different powers levels were tested. As shown in Fig.4, the dependence between efficiency and power follows the behavior predicted by (4).Nevertheless, in the single-frequency RF response, the second maximum of the sinusoidal efficiency curve does not reach the same peak efficiency as the first one. This behavior may be attributed to higher-order acousto-optic interactions, which prevent full power transfer to the first diffraction order, leaving a fraction of the optical power in the zero order.

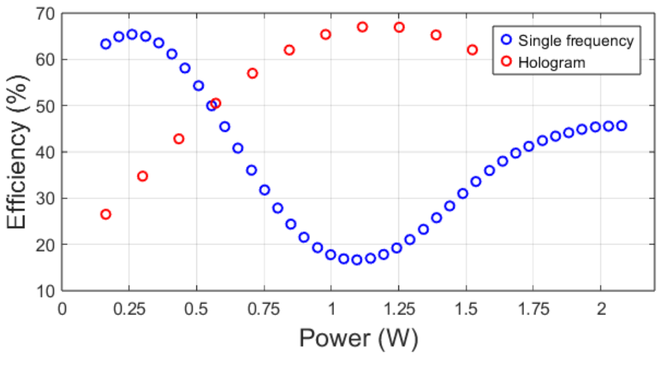

FIG. 4: Saturation curve of the 488 nm beam, for single-frequency and hologram modes.

Figures 6 and 7 (Left) exemplify the behavior outside the Bragg condition. These curves show two frequencies that satisfy equation (3). At these frequencies, the efficiency is given by (4). As the frequency deviates from these values, the efficiency is modulated according to (5). Both the curve shape and the wave vector formalism are similar to those shown in Fig. 1.

Efficiency curves were measured at different power levels. Additionally, the RF response of the transducer was characterized. The RF response (Fig. 6) has its central frequency close to 95 MHz. This curve exhibits a bandwidth and central frequency similar to those of the blue efficiency curve. The transducer was designed to have an RF response with a shape similar to that of the efficiency curves, so the diminishing effect of one on the other is minimized.

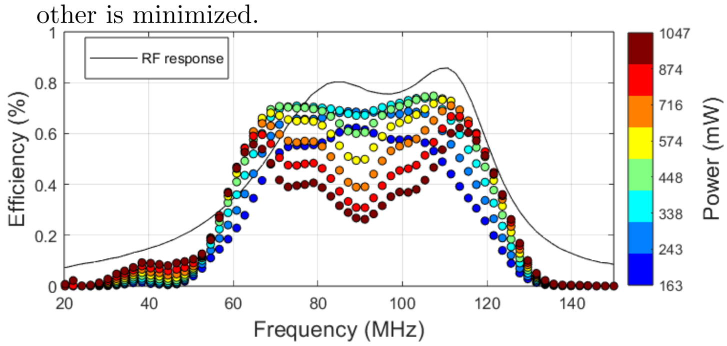

FIG. 6: Efficiency curves for different powers using the 488 nm beam. RF answer curve

The quality of the efficiency curves (Fig. 6) clearly improves as the power approaches the value suggested by the saturation curve. These are the optimal power levels and resulting bandwidths for self-aligned configurations:

	Optimal power (W)		
	Single-frequency	Hologram	Bandwidth (MHz)
488 nm	0.26	1.18	59
561 nm	0.75	1.66	61
637 nm	0.85	>1.66	62

The optimal power for the 637 nm beam exceeds the AOD's maximum input power of 1 W, preventing testing at higher power levels. Even though tests were conducted slightly above 1 W, further increases risked damaging the device. Bandwidth was defined using a 40% efficiency threshold. This criterion was selected because it represents more than half of the specified maximum efficiency (76% according to technical specifications), providing a measure of usable frequency range.

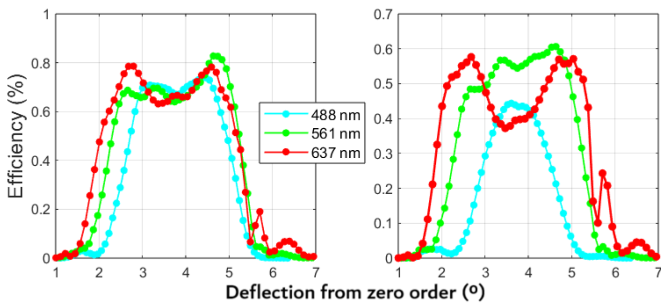

FIG. 7: Left: Efficiency curves self-optimized for each wavelength. Right: Efficiency curves optimized for the 561 nm beam.

For each wavelength, using the optimal alignment and power along with Bragg's law, the angular deflection was measured. The deflection was plotted relative to the zero-order beam. As expected, beams with longer wavelengths

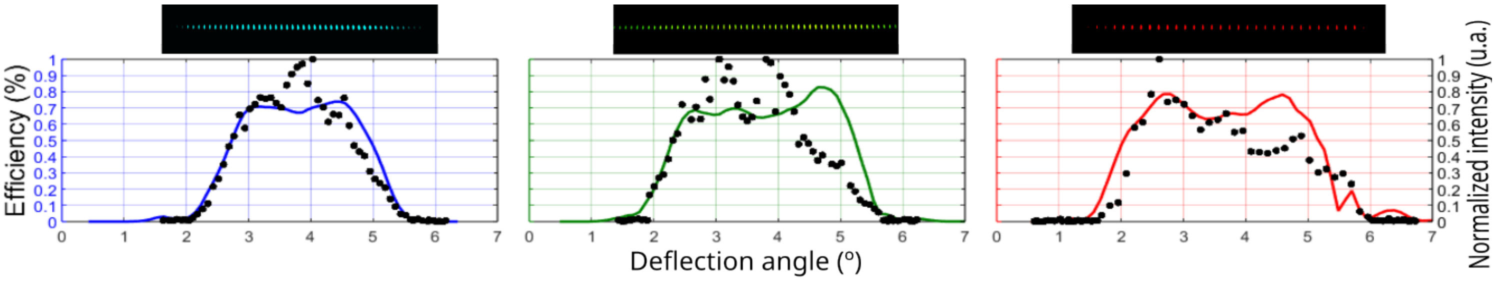

FIG. 5: Hologram intensity profiles and single-frequency efficiency curves under self-optimized alignment conditions.

undergo greater deflection. When measuring the wavelengths of the non-aligned beams, the efficiency plot profile worsens drastically. Despite this, reasonable agreement can be found when aligning to optimize the 561 nm beam (Fig. 7 Right). Even so, in this alignment, the blue beam has a sub-optimal shape and bandwidth.

This suggests that an angle between the 488 nm and 561 nm optimal alignement may exist that would improve the blue curve and serve as a universal alignment for all beams, providing adequate curve shape and reasonable efficiency. However, such an angle was not found. If an optimal alignment valid for all beams is not found, there are two options to work with. The first one is to work with the optimal alignment for every beam(Fig. 7 Left). The second one is to use dichroic mirrors to shift the deflection of only one wavelength.

All previous results were obtained by measuring efficiency at discrete single-frequency points. The Gerchberg–Saxton algorithm was then implemented to create the holograms[4]. Fig.3 shows a superposition of the hologram intensity profile (in arbitrary units) with the efficiency curves for the same wavelength. The hologram efficiency pattern differs from the curves obtained in single-frequency mode, exhibiting variations in shape while maintaining a similar overall bandwidth. Camera-based measurements do not provide direct efficiency values due to setup limitations; therefore, arbitrary units are used, with hologram intensities normalized to a 0-1 scale.

V. UNCERTAINTY ESTIMATION

The RF frequency uncertainty ($\delta f \approx 1$ Hz) is negligible relative to the MHz operating range. Consequently, the angular deflection uncertainty derived from Eq. (3) is also negligible. For the diffraction efficiency $\eta = P_{\text{deflected}}/P_{\text{total}}$, the uncertainty propagates as:

$$\delta\eta = \sqrt{\left(\frac{\delta P_{\text{deflected}}}{P_{\text{total}}}\right)^2 + \left(\frac{P_{\text{deflected}}}{P_{\text{total}}^2}\delta P_{\text{total}}\right)^2} \qquad (8)$$

Using typical low-power values ($P_{\text{total}} = 0.450$ mW, $P_{\text{deflected}} = 0.315$ mW, $\eta = 70\%$ with $\delta P = 0.0005$ mW yields $\delta\eta \approx 0.14\%$, too small to be resolved in the plots. Since these represent the lowest powers employed, the uncertainty remains negligible across all measurements.

VI. CONCLUSIONS

This work has experimentally characterized a rectangular-aperture acousto-optic deflector at 488 nm, 561 nm, and 637 nm, focusing on diffraction efficiency, bandwidth, and wavelength dependence. Distinct optimal incidence angles were identified for each wavelength under broadband excitation, with differences large enough to prevent a common alignment. An alignment optimized at 561 nm provided the closest approximation to a universal configuration, but at the expense of reduced efficiency and bandwidth at 488 nm, highlighting the intrinsic wavelength dependence of rectangular-aperture AOD alignment. The optimal RF power was found to increase with wavelength and to be higher for broadband than for single-frequency excitation, with the 637 nm case exceeding the device's safe operating limits. Measured bandwidths of approximately 60 MHz and the observed efficiency curves are in good agreement with theoretical predictions, providing practical guidelines for wavelength-specific optimization in multi-color scanning systems. This characterization provides valuable data for implementing rectangular-aperture AODs in scanning systems.

Acknowledgments

I would like to thank my advisor, Dr. Jordi Tiana Alsina, for his invaluable dedication and guidance. I am also especially grateful to Jaume Caus for continuous support throughout the laboratory work.

[1] Jieping Xu and Robert Stroud. *Acousto-optic devices: principles, design, and applications*. Wiley, 1992.

[2] Bradley E Losavio, Vijay Iyer, Saumil Patel, and Peter Saggau. Acousto-optic laser scanning for multi-site photostimulation of single neurons in vitro. *Journal of Neural Engineering*, 7(4):045002, 2010.

[3] Kelvin Wagner. Acousto-optic modulators and deflectors. Lecture notes for the Advanced Optics Laboratory, 2018.

[4] R. W. Gerchberg. A practical algorithm for the determination of phase from image and diffraction plane pictures. *Optik*, 35:237–246, 1972.

Caracterització experimental de deflectors acusto-òptics amb finestra rectangular: eficiència, amplada de banda i dependència amb la longitud d'ona

Author: Daniel Eloi Perrella Benítez
Facultat de Física, Universitat de Barcelona

Advisor: Jordi Tiana Alsina

Resum: L'objectiu d'aquest treball és la caracterització d'un deflector acusto-òptic amb finestra rectangular. Aquesta, s'ha fet amb dos tipus diferents de feix làser, un gaussià, com a referència, i un altre el·líptic, que cobreix tota la finestra de l'AOD. A més, s'han fet servir feixos de diverses longituds d'ona (488 nm, 561 nm, 637 nm). S'han mesurat diversos paràmetres del dispositiu: eficiència relativa en funció de la deflexió angular, angles d'incidència òptims, màxima deflexió angular amb certa eficiència (amplada de banda) i, finalment, potència òptima del transductor, per cada longitud d'ona.
Paraules clau: Deflector acusto-òptic, finestra rectangular, feix el·líptic, difracció de Bragg.

ODSs: Educació de qualitat. Indústria, innovació, infraestructures.

Objectius de Desenvolupament Sostenible (ODSs o SDGs)

1. Fi de la es desigualtats		10. Reducció de les desigualtats	
2. Fam zero		11. Ciutats i comunitats sostenibles	
3. Salut i benestar		12. Consum i producció responsables	
4. Educació de qualitat	X	13. Acció climàtica	
5. Igualtat de gènere		14. Vida submarina	
6. Aigua neta i sanejament		15. Vida terrestre	
7. Energia neta i sostenible		16. Pau, justícia i institucions sòlides	
8. Treball digne i creixement econòmic		17. Aliança pels objectius	
9. Indústria, innovació, infraestructures	X		